

# Geometry Optimization using the Frozen Domain and Partial Dimer Approach with the Fragment Molecular Orbital Method: Implementation, Benchmark, and Application for Ligand-Binding Site of Proteins

## *AUTHOR NAMES*

*Koji Okuwaki<sup>1,2,3</sup>, Naoki Watanabe<sup>4</sup>, Koichiro Kato<sup>5</sup>, Chiduru Watanabe<sup>3</sup>, Naofumi Nakayama<sup>6</sup>,  
Akifumi Kato<sup>7</sup>, Yuji Mochizuki<sup>8,9</sup>, Tatsuya Nakano<sup>10#</sup>, Teruki Honma<sup>3</sup>, Kaori Fukuzawa<sup>1,2\*</sup>*

## AUTHOR ADDRESS

<sup>1</sup>Graduate School of Pharmaceutical Sciences, Osaka University, 1-6 Yamadaoka, Suita, Osaka  
565-0871, Japan.

<sup>2</sup>School of Pharmacy and Pharmaceutical Sciences, Hoshi University, 2-4-41 Ebara, Shinagawa-  
ku, Tokyo, 142-8501, Japan

<sup>3</sup>RIKEN Center for Biosystems Dynamics Research, 1-72-22 Suehiro-cho, Tsurumi-ku,  
Yokohama 230-0045, Japan

<sup>4</sup>Mizuho Research & Technologies, 2-3 Kanda Nishiki-cho, Chiyoda-ku, Tokyo 101-8443, Japan

<sup>5</sup>Department of Applied Chemistry, Graduate School of Engineering, Kyushu University, 744 Motooka, Noshi-ku, Fukuoka 819-0395 Japan

<sup>6</sup>CONFLEX Corporation, Shinagawa Center Building 6F, 3-23-17 Takanawa, Minato-ku, Tokyo 108-0074, Japan

<sup>7</sup> Scorpion Tech LLC., 471-5 Okada, Tateyama City, 294-0024, Japan

<sup>8</sup>Department of Chemistry and Research Center for Smart Molecules, Faculty of Science, Rikkyo University, 3-34-1 Nishi-ikebukuro, Toshima-ku, Tokyo 171-8501, Japan

<sup>9</sup>Institute of Industrial Science, The University of Tokyo, 4-6-1 Komaba, Meguro-ku, Tokyo 153-8505, Japan

<sup>10</sup>Division of Medicinal Safety Science, National Institute of Health Sciences, 3-25-26 Tonomachi, Kawasaki-ku, Kawasaki 210-9501, Japan

KEYWORDS. Fragment Molecular Orbital Calculation (FMO), Protein, Ligand-binding site, Frozen Domain method, Geometry optimization.

*\*Corresponding author: Kaori Fukuzawa ([fukuzawa-k@phs.osaka-u.ac.jp](mailto:fukuzawa-k@phs.osaka-u.ac.jp))*

*#Present address: Department of HPC Support, Research Organization for Information Science and Technology, 1-5-2, Minatojima-minamimachi, Chuo-ku, Kobe, Hyogo, 650-0047, Japan*

## ABSTRACT

The frozen domain (FD) approximation with fragment molecular orbital (FMO) method is efficient for partial geometry optimization of large systems. We implemented the FD formulation (FD and frozen domain dimer [FDD] methods) already proposed by Fedorov, D. G. et al. (*J. Phys. Chem. Lett.* **2011**, 2 (4), 282–288.); proposed a variation of it, namely frozen domain and partial dimer (FDPD) method; and applied it to several protein-ligand complexes. The computational time for geometry optimization at the FDPD/HF/6-31G\* level for the active site (six fragments) of the largest  $\beta_2$ -adrenergic G protein-coupled receptor (440 residues) was almost half that of the conventional partial geometry optimization method. In the human estrogen receptor, the crystal structure was refined by FDPD geometry optimization of estradiol, surrounding hydrogen-bonded residues and a water molecule. The rather polarized ligand binding site of influenza virus neuraminidase was also optimized by FDPD optimization, which relaxed steric repulsion around the ligand in the crystal structure and optimized hydrogen bonding. For Serine-Threonine Kinase Pim1 and six inhibitors, the structures of the ligand binding site, Lys67, Glu121, Arg122, and benzofuranone ring and indole/azaindole ring of the ligand, were optimized at FDPD/HF/6-31G\* and the ligand binding energy was estimated at the FMO-MP2/6-31G\* level. As a result, the correlation coefficient between  $pIC_{50}$  and ligand binding energy was considerably improved as compared to results from both molecular mechanics- and quantum mechanics/molecular mechanics-optimized geometries. Thus, this approach is promising as a high-precision structure refinement method for structure-based drug discovery.

## 1. Introduction

The fragment molecular orbital (FMO) method enables quantum chemical calculations of whole bio-macromolecules such as proteins and nucleic acids, yielding the energies and electron densities of whole molecules as well as interaction energies between fragments.<sup>1,2</sup> The FMO calculations of protein complexes whose structures have been experimentally analyzed using X-ray crystallography, nuclear magnetic resonance, and cryo-electron microscopy allow quantitative analysis and physicochemical interpretation of intra- and intermolecular interactions within the complexes. These structural data are obtained from the Protein Data Bank,<sup>3</sup> but these structures generally do not include the coordinates of hydrogen atoms, some structures are missing, and some structures contain unclear coordinates depending on the experimental resolution. Therefore, it is important to refine the experimental structure for precise calculations. Although the classical molecular mechanics (MM) method using molecular force fields is widely used for general molecular modeling, including geometry optimization, the obtained structures depend on the force field parameters and are not always sufficient to describe weak intermolecular interactions, such as hydrogen bonds, halogen bonds, and CH/ $\pi$  interactions. Geometry optimization at the quantum mechanical (QM) level is necessary for more precise structure creation, and several methods have been developed to calculate molecular structure relaxation using the FMO energy and its gradients, such as fully geometry optimization,<sup>4,5</sup> partial geometry optimization (POpt),<sup>6,7</sup> and FMO-based molecular dynamics (MD) methods, such as FMO-MD<sup>2,8,9</sup> and the FMO-QM/MM-MD.<sup>10</sup> These methods have only been applied to a few small proteins in biological systems and have not reached the level of practical use. The density-functional tight-binding combined with the FMO (FMO-DFTB)<sup>11</sup> can be used for whole molecule geometry optimization at low computational cost. However, the accuracy is at the semi-empirical level and there are issues to be solved in the geometry optimization of charged or polarized molecular systems.<sup>12</sup> Therefore, MM energy

minimization is used as a standard preprocessing step for FMO calculations in practice, and QM/MM optimization using the ONIOM method is especially used for precise calculations.<sup>13,14</sup> Recently, a combination of classical molecular dynamics structural sampling and FMO energy calculations was used for energy analyses considering structural fluctuations in water.<sup>15–17</sup>

As the accuracy of interaction analysis using FMO calculations increases, the reliability of the structures used becomes even more important. Experimental structural analysis data (e.g., X-ray crystal structures with a resolution of about 2 Å) may not always provide sufficiently precise structures around the ligand, especially for structure-based drug design (SBDD). Therefore, an approach that optimizes a portion of a large biomolecule is necessary to identify the coordinates of the ligand and its surrounding residues. Although MM calculations are the first choice for biomolecule optimization, there is an imbalance between the MM structures and FMO energies in the evaluation of hydrogen bonds. For example, there is excess charge transfer to the hydrated ligand in the MM structure in some cases,<sup>18</sup> and the correlation of ligand binding predictions with experimental values, such as  $IC_{50}$ ,  $K_i$ , and  $K_D$ , is only obtained after geometry optimization at the QM level in other cases.<sup>13,19</sup> In the example of estrogen receptor (ER), the correlation with the experimental binding values was obtained by optimizing the hydrogen bond distance between the ligand and the hydrogen bonding Glu residue with QM and by appropriately representing the charge transfer between the ligand and the receptor<sup>19</sup>. The activity of serine-threonine kinase Pim1 differs by up to 200-fold for six different chemical structures that only differ in the position of the nitrogen atom in the benzoimidazole ring. We applied several levels of geometry optimization to the complex structures of these compounds and Pim1, evaluated the FMO energy, and reproduced the activity using only QM geometry optimization of the hydrogen bond distance between the

ligand and the residue. Therefore, it is expected that geometry optimization of substructure around the ligand by the FMO method will be an effective approach for precise SBDD.

The first proposal of partial geometry optimization with FMO was reported by Ishikawa et al., namely the partial energy gradient (PEG),<sup>20</sup> wherein the total system was divided into two regions whether the target fragments included ( $R_1$ ) or not ( $R_2$ ), and the gradient was obtained by differentiating the sum of the total energy of  $R_1$  and the interaction energy between  $R_1$  and  $R_2$ . This approach showed that the optimized geometries of prion protein with GN8 molecule and lopinavir with human immunodeficiency virus type 1 (HIV-1) protease by PEG were close to those by conventional method and that the ratios of the computational time of conventional method to that of PEG were around 0.15 for one step of optimization. However, the acceleration by PEG was limited because the electronic structure calculation was the same as conventional FMO. The time-consuming steps of FMO calculation were monomer self-consistent charge (monomer-SCC) process and the following self-consistent field calculation for dimer pairs (dimer-SCF). Tsukamoto et al. implemented the approximation that dimer-SCF calculation of pair consisting of fixed fragments is converted to the dimer-electrostatic (dimer-es) calculation.<sup>7</sup> This approximation is effective for the calculations of the total energy and gradients because the dimer-es term between fixed fragments does not contribute to the semi-analytic gradient of target fragment.<sup>4</sup>

Meanwhile, Fedorov et al.<sup>6</sup> proposed the frozen domain (FD) approximations wherein the system was separated by three domains: active, polarizable buffer and frozen. These approaches reduce the number of dimer-SCF pairs and the number of fragments updating the electronic structure on each optimization step by monomer-SCC. Frozen domain dimer (FDD) approximations succeeded in saving the computational cost of the entire FMO calculation for partial geometry optimization. Nakata and Fedorov<sup>21</sup> implemented FD and FDD combined with

the polarizable continuum model (PCM) and the acceleration factor comparing FMO/FDD to full FMO was 38 and 12 for Trp-Cage (PDB: 1L2Y) with 161 water molecules and crambin (PDB: 1CRN), respectively. FMO/FDD/PCM was also applied to the partial geometry optimization of the ligand and binding pocket of K-Ras (PDBID: 4Q03).

In this study, we propose a novel approach based on the FD framework, namely “frozen domain and partial dimer (FDPD)” and implemented it with FD and FDD into ABINIT-MP program.<sup>2,22</sup> The accuracies of the methods were evaluated on chignolin and Trp-Cage comparing semi-analytic and numerical gradients. The methods were also applied to the complex of human ER ligand binding domain with 17 $\beta$ -estradiol, complex of N1 neuraminidase (NA) with oseltamivir carboxylate, the complex of  $\beta_2$ -adrenergic G protein-coupled receptor with the ligand ( $\beta_2$ AR; for benchmark only), and Pim1 kinase with six compounds.

## 2. COMPUTATIONAL DETAILS

### 2.1 Energy Definition

In the FD framework, the total system was divided into the three domains (Figure 1): the active domain (L3), which included the fragments to be optimized; the buffer domain (L2) around L3 fragments; and the FD (L1). The total FMO energy of the FD approach is:

$$E^{\text{FMO/FD}} = \sum_{I \in \text{L1}} E'_I + \sum_{I \in (\text{L2}+\text{L3})} E'_I + \sum_{\substack{I > J \\ I, J \in (\text{L2}+\text{L3})}} \Delta E_{IJ} + \sum_{\substack{I \in \text{L3} \\ J \in \text{L1}}} \Delta E_{IJ} \quad (1)$$

$$\Delta E_{IJ} = \Delta E'_{IJ} + \text{Tr}(\Delta \mathbf{D}^{IJ} \mathbf{V}^{IJ}) \quad (2)$$

$$\Delta E'_{IJ} = E'_{IJ} - E'_I - E'_J \quad (3)$$

where  $E'_I$  and  $E'_{IJ}$  are the internal monomer and dimer energies, respectively.  $\Delta \mathbf{D}^{IJ}$  and  $\mathbf{V}^{IJ}$  are the dimer density difference and electrostatic potential matrices, respectively. The electronic

structures of fragments in L1 were obtained once in the initial geometry and were unchanged during the preset cycle of optimization (keyword “OptDefrozeInterval” in ABINIT-MP). Therefore, the first term in Eq. (1) was constant and its gradient was zero.

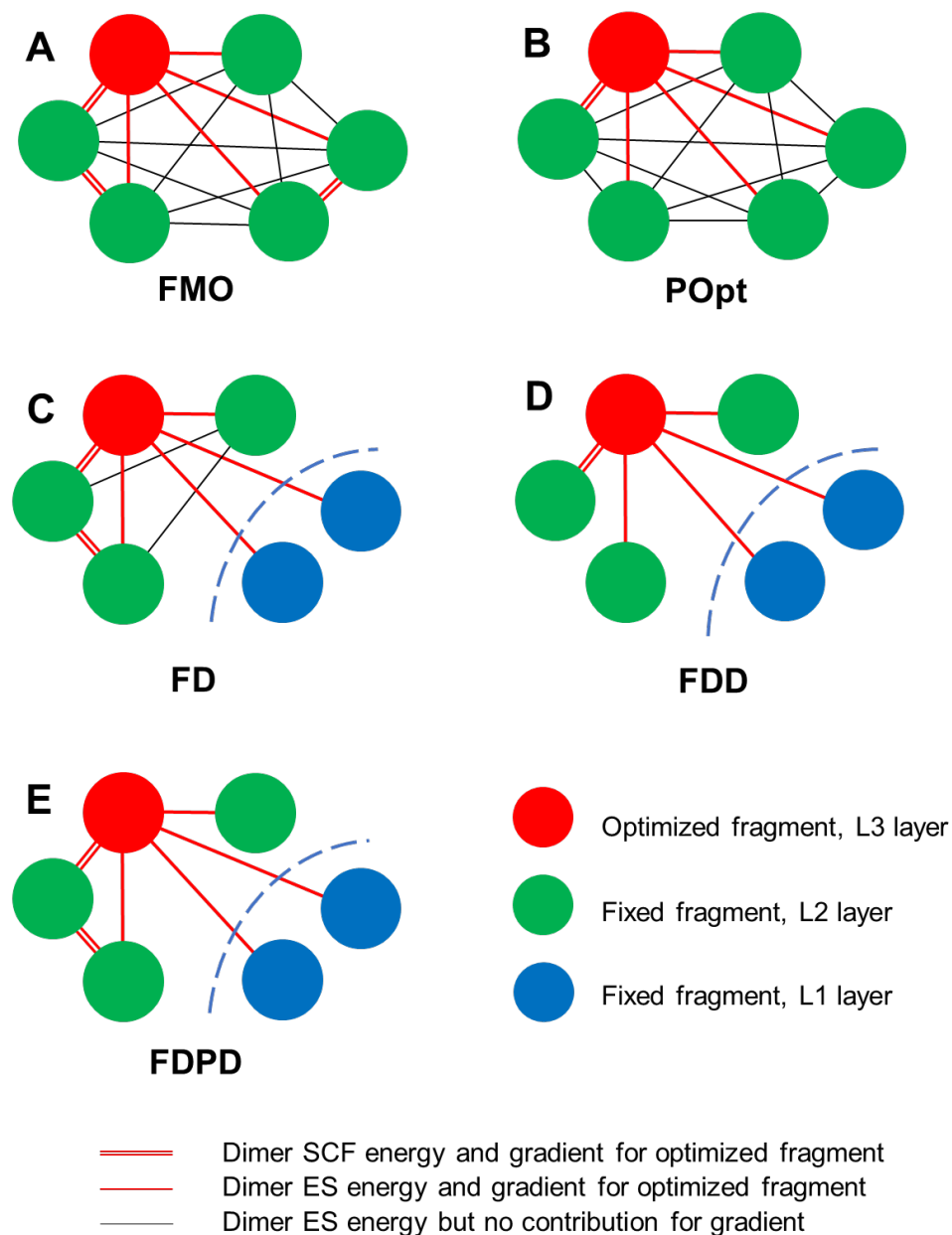


**Figure 1.** Schematic representation of dimer interactions contributed to energy and gradient in each method. (A) Full FMO optimization,<sup>4</sup> (B) Partial geometry optimization implemented in 2013 (POpt),<sup>6,7</sup> Partial geometry optimization with (C) Frozen domain (FD), (D) Frozen domain and dimer (FDD), and (E) Frozen domain and partial dimer (FDPD) approximations.

Further approximation to speed up the calculation of energy and gradient (referred to as FDD) included neglecting the dimer energies between fragments in L2. The total FMO/FDD energy is as follows:

$$E^{\text{FMO/FDD}} = \sum_{I \in \text{L1}} E'_I + \sum_{I \in (\text{L2+L3})} E'_I + \sum_{\substack{I > J \\ I \in \text{L3}, J \in (\text{L2+L3})}} \Delta E_{IJ} + \sum_{\substack{I \in \text{L3} \\ J \in \text{L1}}} \Delta E_{IJ} \quad (4)$$

However, the dimer interactions close to L3 fragments should not be neglected for optimization. The gradients of these interactions obtained by dimer-SCF calculation can be computed based on ref.<sup>4</sup>. Consequently, we determined the total energy of new FDPD approach as:

$$E^{\text{FMO/FDPD}} = \sum_{I \in \text{L1}} E'_I + \sum_{I \in (\text{L2+L3})} E'_I + \sum_{\substack{I > J \\ I \in \text{L3}, J \in (\text{L2+L3})}} \Delta E_{IJ} + \sum_{\substack{I > J \\ I, J \in \text{L2}}} \Delta E_{IJ}^{\text{dimer-SCF}} + \sum_{\substack{I \in \text{L3} \\ J \in \text{L1}}} \Delta E_{IJ} \quad (5)$$

The gradients of initial geometry under the FDPD approach were the same as those in the FD approach because the gradients of dimer interactions in L2 based on dimer-es calculation were not included.<sup>4</sup>

## 2.2 Domains for Target Systems

In ABINIT-MP program,<sup>2,22</sup> the thresholds of approximations to the two-electron electrostatic potential (“esp-aoc” and “esp-ptc”) and the threshold of dimer-es approximation are given in unit of the van der Waals (vdW) radius.<sup>23</sup> For example, the default threshold value of dimer-es approximation (keyword “Ldimer”) is 2.0. This value means that threshold distance for dimer-es approximation was 2.0 times the sum of the vdW radii of the shortest contact atoms between monomers. We implemented new keyword “Lbuffer,” which is the threshold for specifying the L2 domain. The default value of “Lbuffer” is 2.0, and it works the same way as “Ldimer” wherein the

threshold is 2.0 times the sum of the vdW radii of the shortest interatomic distance between the monomer in the L3 domain and another monomer. The domain definitions of target proteins are shown in Figure 1.

Partial geometry optimizations were performed using the Broyden-Fletcher-Goldfarb-Shannon (BFGS) scheme.<sup>24</sup> The thresholds of optimizations were 0.01 and 0.007 hartree/bohr for the maximum and root-mean-square (RMS) gradient values, respectively, and 0.02 and 0.014 bohr for the maximum and RMS displacements, respectively (these are default values in ABINIT-MP).

### 2.3 Target Systems

The calculation targets are shown in Figure 2, and the fragments in L3 domain are listed in Table 1. Chignolin (PDBID: 1UAO) and Trp-Cage (PDBID: 1L2Y) were used for semi-analytic gradient validation, while the ER truncated model (89 fragments), ER (243 fragments, PDBID: 1ERE), N1 neuraminidase (NA) (378 fragments, PDBID: 2HU4), and  $\beta_2$ AR (441 fragments, PDBID: 2RH1) were utilized for speed benchmarking. The same ER and NA, as well as Pim1 (271 fragments, PDBID: 5VUC) were calculated as application targets. The ligands of the complex for ER, NA,  $\beta_2$ AR, and Pim1 were 17 $\beta$ -estradiol, oseltamivir carboxylate, (S)-carazolol, and six benzofuranone-class inhibitors, respectively. The fragment IDs of the L3 region are listed in Table S1. In these calculations, molecular operating environment (MOE) software<sup>25</sup> (Chemical Computing Group) was used to model all structures, employing either the MMFF94x<sup>26</sup> or Amber99<sup>27</sup> or Amber10:EHT<sup>28,29</sup> force field. Subsequently, geometries were optimized at the FMO-HF/6-31G\* level in FD framework and the interaction energies were re-evaluated at the FMO-MP2/6-31G\* level<sup>30,31</sup> for the optimized structure using ABINIT-MP program.<sup>2,22</sup> Details of these will be discussed in each section. The FMO calculation results of FMO-optimized

structures and the related data, such as X-ray and the modeling structure by MM and QM/MM methods, were registered in FMO database,<sup>32,33</sup> and their entry IDs (FMO DB IDs) are listed in Table S2.

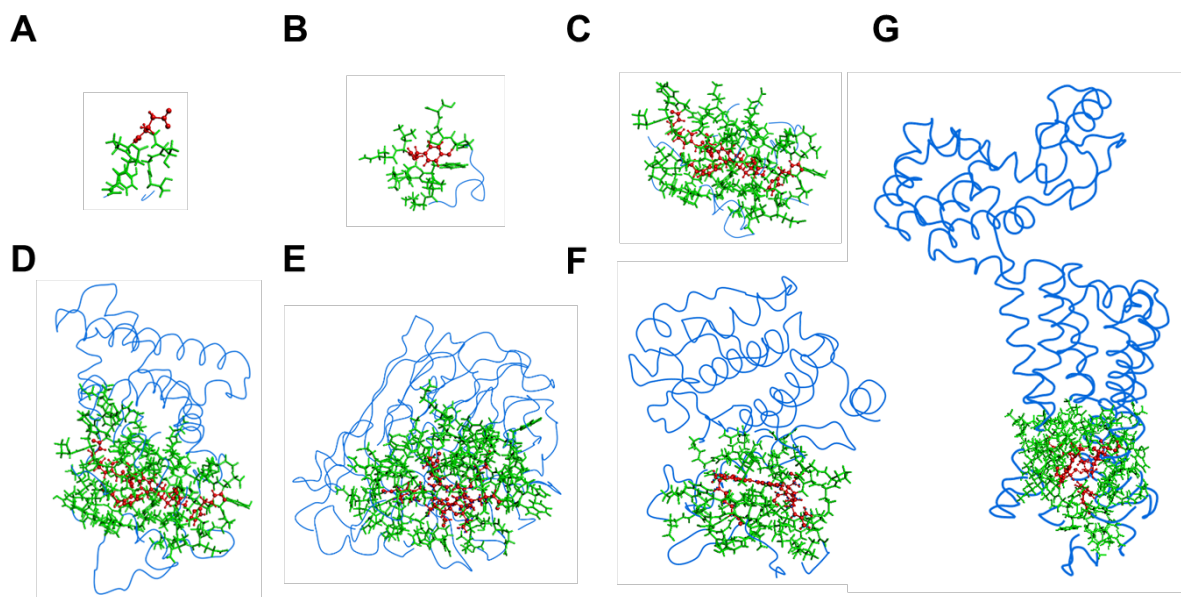


Figure 2. Frozen domain regions of target systems. Red, green, and blue indicate L3, L2, and L1, respectively. (A) Chignolin, (B) Trp-Cage, (C) ER truncated model, (D) ER, (E) NA, (F) Pim1, and (G)  $\beta_2$ AR.

Table 1. Fragments in L3 and their residues or molecules for each protein (Figure 2).

Protein	Residue or molecule
(A) Chignolin	Glu5
(B) Trp-Cage	Tyr3
(C) ER truncated model	Glu353, Arg394, Phe404, His524, Water, Ligand
(D) ER	Glu353, Arg394, Phe404, His524, Water, Ligand
(E) NA	Arg118, Arg292, Tyr347, Arg371, Ligand
(F) Pim1	Lys67, Glu121, Arg122, Ligand*
(G) $\beta_2$ AR	Asp113, Val114, Phe193, Ser203, Asn312, Ligand

\* The ligands were split into two parts, with only one part set as the L3 region (see Figure 6c).

### 3. RESULTS AND DISCUSSION

#### 3.1. Accuracy of Semi-Analytic Gradient

Differences between semi-analytic and numerical gradients for Chignolin and Trp-Cage in each method are shown in Table 2. Those of FMO and POpt methods are also included for comparison. The accuracy of our FDPD was better than those of POpt and FDD and was quite similar to that of FD. Computational details for optimization and the total energies of optimized structures are summarized in Table S3.

Table 2. Root-mean-square deviation (RMSD) and maximum difference between semi-analytic and numerical gradients for Chignolin and Trp-Cage. Serial numbers of optimized atoms were 45, 46, 57, and 61–71 for Chignolin and 34–37 and 39–54 for Trp-Cage.

Protein	Basis set	Method	RMSD	Max. error	
Chignolin	6-31G	FMO	0.001727	0.005319	
		POpt	0.001857	0.005512	
		FD	0.001769	0.005190	
		<b>FDPD</b>	0.001760	0.005116	
		FDD	0.003183	0.013836	
		6-31G*	FMO	0.001189	0.004585
	POpt		0.001647	0.004001	
	FD		0.001280	0.004770	
	<b>FDPD</b>		0.001279	0.004821	
	FDD		0.003311	0.014548	
	Trp-Cage		6-31G	FMO	0.001076
		POpt		0.001641	0.004788

FD	0.001222	0.003077
<b>FDPD</b>	0.001208	0.002202
FDD	0.002550	0.004337

---

### 3.2 Performances of FD Approximations

To investigate the acceleration, a comparison of the computational time for one optimization cycle in the POpt, FD, FDPD, and FDD methods was performed for proteins of different sizes. The target molecules were the ER truncated model,<sup>34</sup> ER, NA, and  $\beta_2$ AR (Figure 2). In addition to the ligand molecule, the residues to be optimized were set to the surrounding four residues and a water molecule for ER, the surrounding four residues for NA, and the five residues for  $\beta_2$ AR, with 1112, 1179, and 1117 atomic orbitals for the respective optimized regions. The system size significantly increased in POpt without the FD, whereas the increase was suppressed when the FD was applied, and the performance of FDD was increased 1.94 times compared to its POpt.

Notably,  $\beta_2$ AR exhibited a reduction in computation time across all three FD types when compared to NA despite having a higher total number of fragments. The number of fragments for each layer, dimer-SCF, and dimer-es across all targets is shown in Table S4. While the number of fragments in the L3 region was higher for  $\beta_2$ AR than for NA (6 compared to 5 for  $\beta_2$ AR),  $\beta_2$ AR had fewer fragments in the L2 region (52 compared to 74 for NA). Consequently, the total number of dimer-SCF in regular FMO was similar for both (3217 for NA and 3213 for  $\beta_2$ AR), but the numbers were 492 for NA and 333 for  $\beta_2$ AR in FDPD, with a significant reduction observed in  $\beta_2$ AR. The number of dimer-es in FDPD was higher for  $\beta_2$ AR (2517 compared to 1766 for NA), but the total computation time was shorter for  $\beta_2$ AR. These results suggest that the total number of dimer-SCF (which is dependent on the L2 region) had a more significant impact on the total computation time than the total number of fragments or the L3 region.

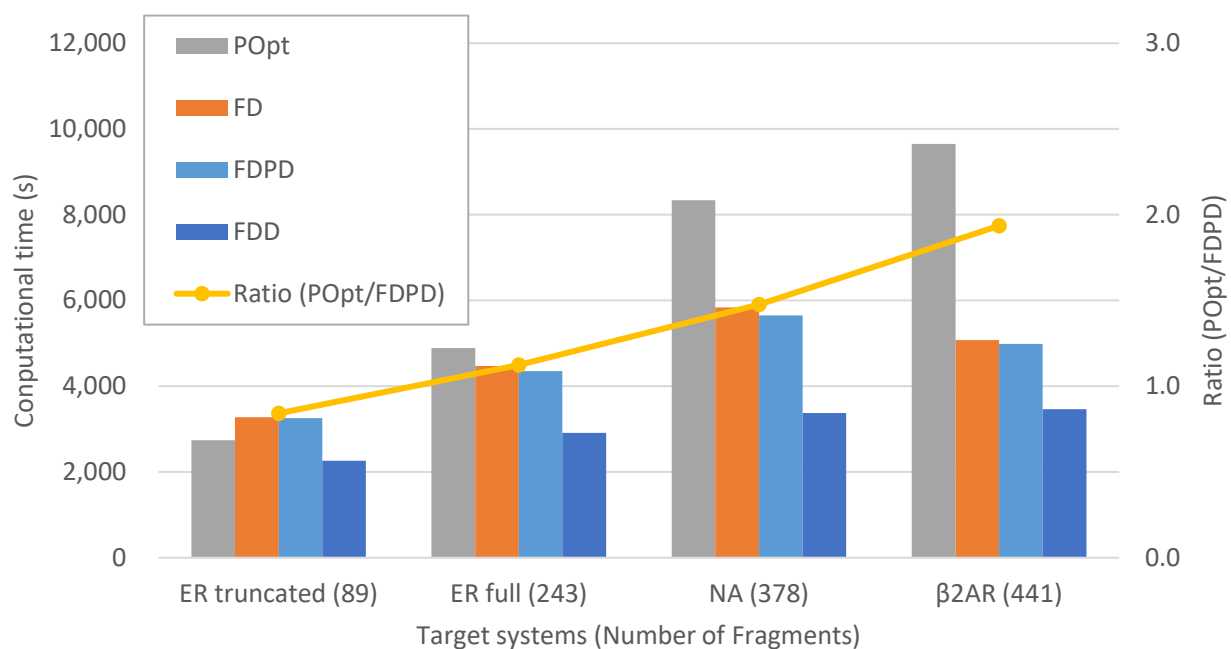


Figure 3. Computational time per cycle of frozen domain geometry optimization. Comparison between POPT and FD methods. Calculations were performed on 112 cores of a Xeon-based house server (Intel Xeon(R) Gold 6238R) owned by the research group, with 5 GB of memory per core and 4 CPUs allocated per fragment.

### 3.3 Applications for Biomolecules

The formation of intermolecular hydrogen bonds and CH/ $\pi$  bonds is important for the molecular recognition of biological systems. Specific hydrogen bonds are often formed in the ligand-binding pocket, especially in ligand recognition. Here, we optimized the hydrogen bond network by partial geometry optimization and validated the effectiveness of this approach for three important drug discovery targets: nuclear receptor, neuraminidase, and kinase, as examples of protein–ligand binding.

#### 3.3.1 Estrogen Receptor

Initially, we applied three optimization methods (FD, FDD, and FDPD) to a complex of the human estrogen receptor (ER)  $\alpha$  ligand binding domain, a member of nuclear receptor superfamily,

with 17 $\beta$ -estradiol (PDBID: 1ERE). X-ray crystallography and FMO calculations revealed that the ligand had two hydroxyl groups, the first forming a hydrogen bond network with Glu353, Arg394, and a crystal water, and the second forming a hydrogen bond with His524. Optimization of these hydrogen bond structures at the QM level was necessary to obtain a correlation between the calculated binding energy and the experimental relative binding affinity.<sup>19</sup> However, the geometry optimization calculations at the HF/6-31G\* level in 2005 could not handle large protein structures; therefore, a small model only consisting of the hydrogen bonding substructure (ligand, some amino acid residues, and crystal water was used).<sup>19</sup> In the 2013 geometry optimization of protein substructure at the FMO-HF/6-31G\* level, the model structure was truncated to the ligand and 87 surrounding residues (truncated model).<sup>34</sup> Finally, it was possible to perform partial geometry optimization using the entire protein-ligand complex model with the implementation of FMO/FD calculations. Here, we validated the results of the FD optimization calculations, including comparison with previously calculated structures. We started with an initial structure in which the hydrogen direction of the -OH group, the donor of the hydrogen bond with His524, was reversed to confirm the efficacy of the FD geometry optimization.

The important interatomic distances in the structures obtained using the three optimization methods are shown in Table 3. The optimized structures obtained using all methods are similar. The extremely short hydrogen bond distance between Glu353 and ligand (1.34 Å) observed in the initial structure, wherein the coordinates of the heavy atoms were fixed at the crystal structure, was corrected to around 1.6 Å by the geometry optimization. It was one of the shortest hydrogen bond distances, suggesting that the hydrogen bond was strong. Meanwhile, the other hydrogen bond distances formed with Arg394 and His524 were approximately 2.1 Å, indicating that they are moderate hydrogen bonds. Focusing on the O-H covalent bond distances of the hydroxy groups

involved in these hydrogen bond networks, the distance on the Glu353 side was 0.98 Å, which was longer than that of His524 (0.96 Å). This indicated that the weakly acidic proton of phenol was "slightly attracted" by the carboxy group of Glu. Furthermore, the fact that the hydrogen bond distance between the other hydroxy group and His524 (which was placed in the opposite direction in the initial structure) was properly optimized from 2.8 Å to 2.1 Å indicated that the partial geometry optimization was functioning properly.

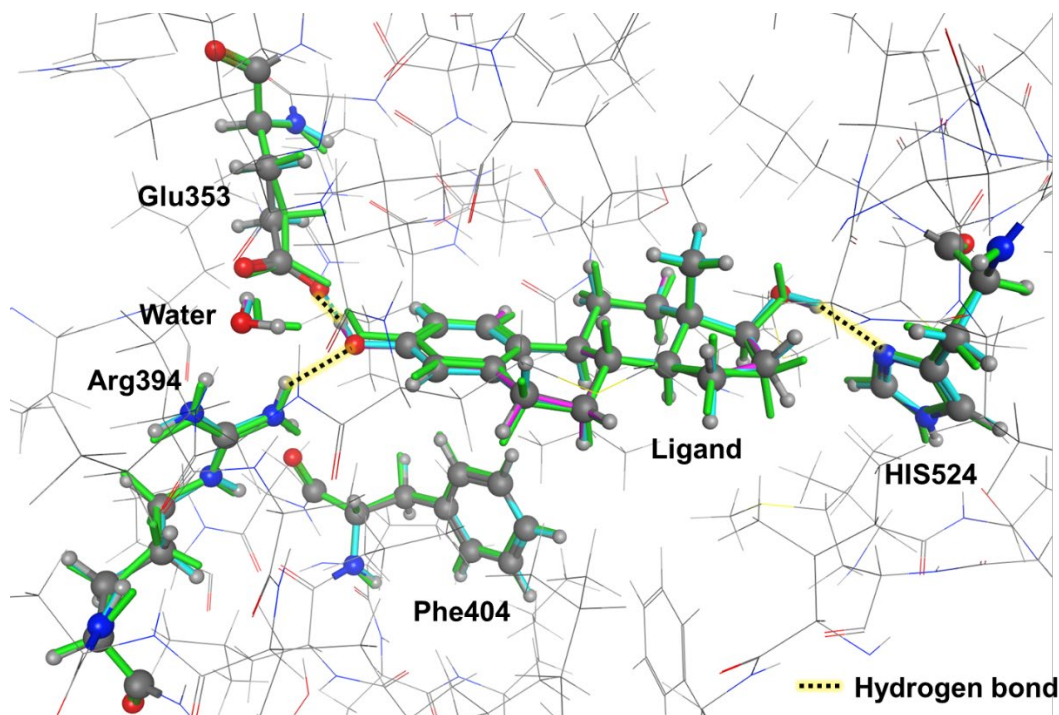


Figure 4. Molecular structure of the ligand and surrounding amino acids. Green, magenta, cyan, and atomic colors represent the initial, FD-, FDD-, and FDPD-optimized structures, respectively. The stick model indicates the atoms in the L3 region. The line model indicates the atoms in the L2 and L1 regions.

Table 3. Various interatomic distances in ER (Å).

Geometry	GLU353-ligand	ARG394-ligand	His524-ligand	Ligand A-OH*	Ligand D-OH*
<b>Initial<sup>#</sup></b>	1.349	2.250	2.803	1.000	0.948

<b>POpt</b> <sup>34, #</sup>	1.601	2.153	2.063	0.986	0.959
<b>FD</b>	1.643	2.079	2.101	0.979	0.953
<b>FDPD</b>	1.640	2.078	2.104	0.979	0.959
<b>FDD</b>	1.607	2.029	2.168	0.986	0.964

\*Covalent O-H bond distance, #Truncated model was used.

The inter-fragment interaction energy (IFIE) between the ligand and surrounding residues obtained from these optimized structures are shown in Table 4. The interaction energy values obtained by all methods were similar from the generally comparable structures. First, the IFIE between the ligand and His524 was significantly stabilized from +3.3 in the initial structure to around -14 kcal/mol with the formation of a hydrogen bond between them. The summation of IFIE (IFIE Sum) between the ligand and the residues, which corresponds to the binding energy, was also greatly stabilized by the formation of this hydrogen bond. The IFIE with Glu353 was approximately -34 kcal/mol, which was more energetically stable than that of His524. In these cases, the hydrogen bond distances corresponded to the strength of interaction energy, but in some cases, [such as Arg394 (about 6 kcal/mol) and His524] the interaction strengths were different even at comparable hydrogen bond distances. In other words, precise structure and quantitative energy evaluation are important to reveal the quantity and quality of intermolecular interactions.

Table 4. Interaction energies between the ligand and its surrounding fragments in ER evaluated at the MP2/6-31G\* level of theory (in kcal/mol).

<b>Geometry</b>	<b>GLU353</b>	<b>ARG394</b>	<b>PHE404</b>	<b>His524</b>	<b>Water</b>	<b>IFIE Sum</b>
<b>Initial</b> <sup>#</sup>	-33.2	-9.0	-5.1	3.3	-2.4	-86.5
POpt	-36.6	-4.5	-5.4	-15.3	-1.5	-107.7
FD	-34.2	-6.1	-5.5	-14.2	-1.3	-106.6

FDPD	-34.0	-6.1	-5.5	-14.3	-1.3	-106.5
FDD	-34.9	-6.4	-5.6	-13.8	-1.6	-107.7

<sup>#</sup>Truncated model was used.

### 3.3.2 Influenza Virus Neuraminidase

In the second example, partial geometry optimization was performed for the complex structure of influenza virus NA and the anti-influenza drug oseltamivir<sup>18,34,35</sup>; as oseltamivir carboxylate is a zwitterion, this is an example of geometry optimization of an intermolecular ion pair in a highly polarized ligand-binding pocket. The negatively charged carboxy groups formed ionic interactions with the surrounding basic residues, such as Arg371, Arg292, and Arg118, while the positively charged amino groups formed similar electrostatic interactions with the surrounding acidic residues, such as Glu119 and Asp151. However, only the residues on the above carboxy group side of the NA residues were considered as the optimized region. In the model of NA described in Section 3.2, we compared the crystal structure to the structures obtained from the FDPD optimization. Figure 5 illustrates the initial structure<sup>35</sup> superimposed on the various optimized structures. Moreover, Table 5 presents the initial and the FDPD optimized structure, specifically the distance information between the ligand and the principal residues; the IFIE and PIEDA values before and after geometry optimization are shown in Table S5. Upon FDPD calculation, Arg118 and Tyr347 were found to have shorter distances and stronger interaction than those of initial structure, while Arg371 had longer distances and weaker interaction. The distance between the hydrogen atom HH22 of Arg371 and the carboxy oxygen atom O1B of the ligand increased from 1.7 Å to 1.8 Å, suggesting that the exchange repulsion (EX) value in the FMO calculation weakened and the structural repulsion was alleviated. The weakened EX value in the FMO calculation signifies that the structural repulsion was effectively eliminated. Thus, the ionic hydrogen bonding network was moderately optimized.

Table 5. Initial and FDPD optimized structure distance information between key ligand residues. Values in parentheses are those in the initial structures.

Pocket residue	Pocket atom	Ligand atom	Distance / Å	IFIE / kcal/mol
ARG118	HH11	O1B	2.408 (2.696)	-15.7 (-12.3)
ARG118	HH22	O1B	2.706 (2.980)	
ARG371	HH22	O1B	1.839 (1.702)	-84.5 (-91.8)
ARG371	HH11	O1A	1.803 (1.699)	
ARG292	HH12	O1A	2.118 (2.106)	-39.3 (-40.2)
ARG292	HH22	O1A	2.540 (2.563)	
TYR347	HH	O1A	2.031 (2.083)	-14.3 (-9.7)

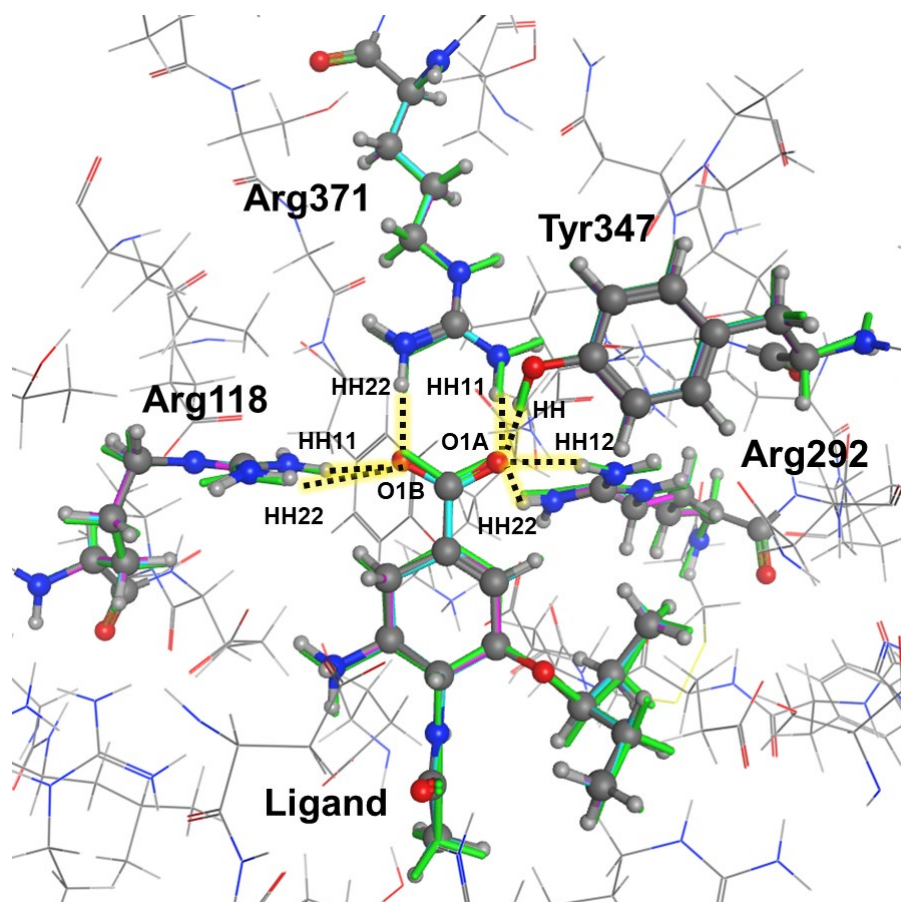
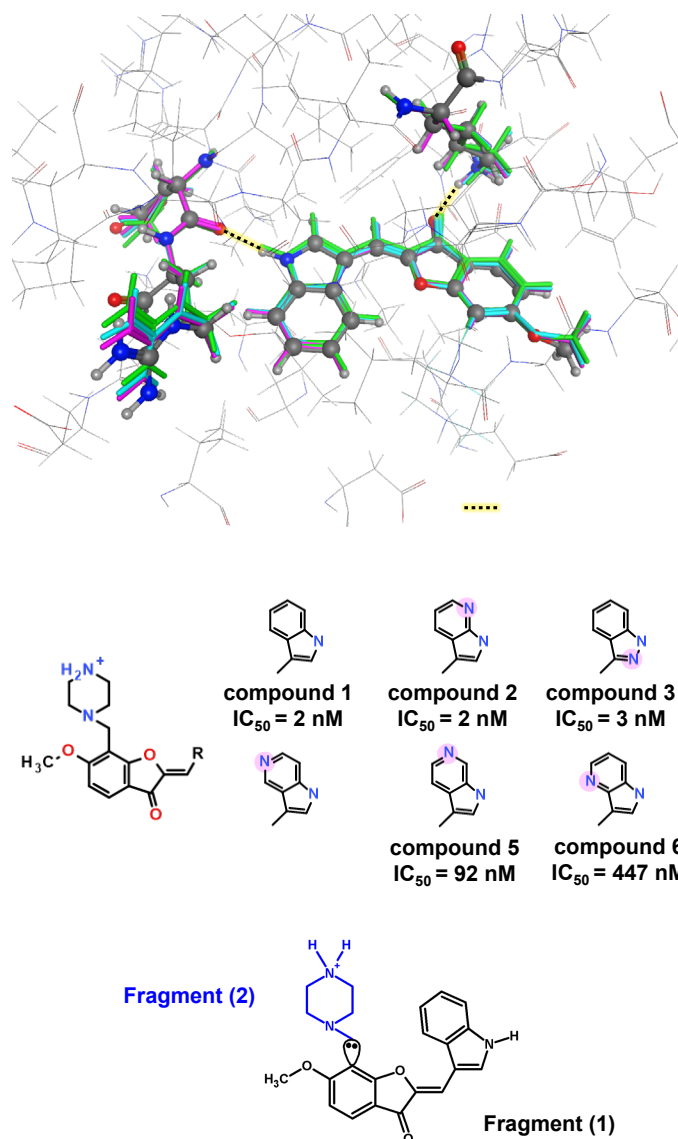


Figure 5. NA ligand (G39) and surrounding residues. Green, magenta, cyan, and atom color represent initial structure, FD, FDD, and FDPD results, respectively. The stick model indicates the atoms in the L3 region; The line model indicates the atoms in the L2 and L1 regions.

### 3.3.3 Predicting the Inhibitory Activity of Pim1 Kinase

In the last example, we predicted inhibitory activity of Pim1 Kinase, comparing MM, QM/MM, and FMO-optimized structures. In a previous study<sup>13</sup> that examined the prediction of inhibitory activity relationships for Pim1 kinase and its inhibitors that exhibited activity cliff based on FMO calculations. To determine if the different structures used in the FMO calculations affect the activity prediction, we compared FMO results for three different structures: X-ray crystal structures of each complex, and MM- or QM/MM-optimized structures based on modeling structures from a single template complex. The results showed that the modeling structure using the same template (Figures 2F and 6A) was suitable for predicting notable changes in activity values owing to slight structural differences, such as activity cliffs (Figure 6B).<sup>13,36</sup> Furthermore, the QM/MM-optimized structures had the best correlation between experimental inhibitory activities and predicted inhibitor binding energies. Therefore, we compared the inhibitory activity relationship in the MM-, QM/MM-, and FMO-optimized structures using the template model to confirm the usefulness of the FMO-based geometry optimization developed in the present study, which treats the entire system with QM calculations.



**Figure 6.** Complex between Pim1 kinase and compound 1 (A). The stick model indicates the atoms in the L3 region; The line model indicates the atoms in the L2 and L1 regions. The FMO-optimized structure with FDPD is indicated by color for each element type. The FMO-optimized structures with FD and FDD are shown in magenta and cyan, respectively. The X-ray crystal structure is shown in green. Benzofuranone-class Pim1 kinase inhibitors and its inhibitory activity values  $IC_{50}^{36}$  (B). Fragmentation of inhibitor (C).

The flows of each geometry optimization using MM, QM/MM, and FMO methods are explained in Supplementary Information section 4. Note that each method has a different optimization region,

as shown in Figure S1; FMO optimization (Fig S1C) allows for a wider optimization region. The FMO geometry optimizations were performed by FD, FDPD, and FDD approaches, where each residue was treated as different fragments and the inhibitor was divided into two fragments, as shown in Figure 6C.

Details of the FMO geometry optimization calculation with FD, FDPD, and FDD methods and the subsequent FMO-MP2/6-31G\* single point calculation are shown in Supplementary Information section 4 and Tables S6–S10. Hydrogen bond distances,  $r_1$  and  $r_2$  (Figure S1) were increased by QM optimization: the distances of the QM/MM- and FMO-optimized geometries were prolonged on average by 0.1 and 0.2 Å when compared with those of the MM, respectively (Tables S7–S10). Although the difference in theoretical levels did not significantly affect the IFIE between the inhibitor and its hydrogen-bonding fragment of Pim1 (Glu121 and Lys67), the FMO geometry optimization moderated the interaction energies of the ES and EX components. In particular, the exchange repulsion was contained at approximately 10 kcal/mol.

Subsequently, inhibitor binding energy between Pim1 kinase and each inhibitor was estimated using each modeling structure. Here, the inhibitor binding energy  $\Delta E_{\text{compound } X}$  was a summation of IFIEs over Pim1 kinase with compound  $X$  ( $X = \mathbf{1} \sim \mathbf{6}$ ). Figure 7 shows the correlations between the experimental inhibitory activity ( $\text{pIC}_{50} = -\log_{10} [\text{IC}_{50}]$ ) and referential inhibitor binding energy; the referential inhibitor binding energies in the cases of MM, QM/MM, and FMO geometry optimizations were the differences from a reference value of compound **1** with FMO geometry optimization at the FDPD/HF/6-31G\* level.

$$\Delta\Delta E_{\text{inhibitor}} = \Delta E_{\text{compound } X} - \Delta E_{\text{compound } \mathbf{1}}; X = \mathbf{2} - \mathbf{6}. \quad (6)$$

The results of the FMO geometry optimization at the FDPD level showed the best correlation with the experimental values (Figure 7C). Correlation coefficients  $R^2$  between  $pIC_{50}$  and  $\Delta\Delta E_{\text{inhibitor}}$  based on results of MM, QM/MM, and FDPD optimized geometries were 0.58, 0.67, and 0.81, respectively. The correlations improved by increasing the QM region for geometry optimization. The FDPD method can optimize more atoms at the QM level than the QM/MM method, and the entire molecular system can be treated in the QM level, thus improving the prediction of inhibitory activity significantly.

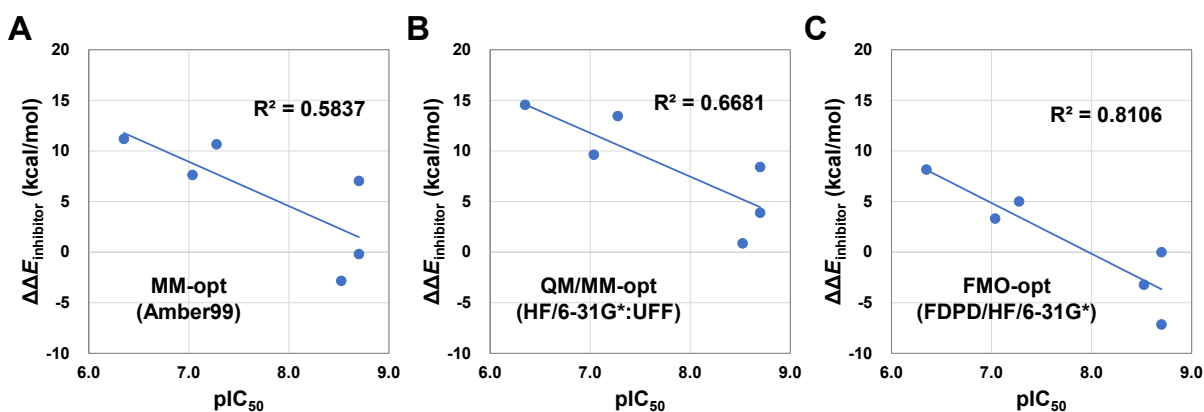


**Figure 7.** Correlation between  $pIC_{50}$  and the referential inhibitor binding energies  $\Delta\Delta E_{\text{inhibitor}}$  using a reference value of compound **1** ( $\Delta E_{\text{compound 1}} = -473.8$  kcal/mol); Geometry optimization methods are MM with Amber99 force field (A), QM/MM at HF/6-31G\*:UFF level (B), and FMO with FDPD at HF/6-31G\* level (C).

#### 4. CONCLUSIONS

The FD framework for partially optimization (FD, FDD, and FDPD) was implemented into the ABINIT-MP program, and the accuracy of gradients and the computational time per optimization cycle was compared. The error of the gradients between analytical and numerical methods of FDPD was close to those at FMO and FD and were smaller than those at POpt and FDD. The average time of each optimization cycle for FDPD were slightly longer than those for FD. The FD

optimization successfully refined the initial crystal structure. In particular, examples of structural refinement of hydrogen bonding networks in the ligand-binding pockets of proteins were demonstrated using protein-ligand complexes, such as ER and NA. This helps improve structural uncertainties around the ligand in the crystal structure. Notably, these advancements were not achieved by truncating only the pocket region structure but performing all-electron calculations on the entire protein structure.

The prediction of inhibitory activity of Pim1 kinase was demonstrated: geometry optimization of the active site using the FD framework depicted higher accuracy in correlation with  $pIC_{50}$ , even more than that found using QM/MM method. These results suggest that this approach can be a highly accurate SBDD method. The practical application of this geometry optimization is expected to be the first step toward elucidating chemical reactions (especially enzymatic reaction mechanisms which are expected from quantum chemical calculations of biological systems) and this should be further explored in future research.

## ACKNOWLEDGMENT

The authors thank Dr. Dimitri G. Fedorov of the National Institute of Advanced Industrial Science and Technology for discussions on FMO geometry optimizations. The authors also thank Prof. Kazuo Kitaura of Osaka University, Dr. Yuto Komeiji of the National Institute of Advanced Industrial Science and Technology, and Dr. Yoshio Okiyama of Kobe University for general discussions related to FMO calculations. FMO DB: Dr. Kikuko Kamisaka of RIKEN for technical support of FMO DB registration for the optimization data. This study was partly supported by the Platform Project for Supporting Drug Discovery and Life Science Research (Basis for Supporting Innovative Drug Discovery and Life Science Research) (BINDS) from the Japan Agency for

Medical Research and Development (AMED) (Grant Numbers JP21am0101113 and JP24ama121030), Interdisciplinary Cutting-edge Research from the AMED (Grant Number 23wm0325063h0001) and by JSPS KAKENHI (Grant Number 21K05105). This research was performed as an activity of the FMO drug design consortium (FMOODD). A part of the FMO calculations were performed using the supercomputer Fugaku (project ID: hp230131) and SQUID at the Cybermedia Center, Osaka University. We would like to thank Editage ([www.editage.jp](http://www.editage.jp)) for English language editing.

#### Data and Software Availability

All structure files and a set of input/output files used for FMO calculations are available at the FMOODB (<https://drugdesign.riken.jp/FMOODB/>); FODB IDs are listed in Table S2. Simple data analysis can be performed using the FMOODB web interface, and detailed analysis can be performed using the BioStation Viewer software (<https://fmodd.jp/biostationviewer-dl/>). FMO Software ABINIT-MP was pre-installed on high-performance computing infrastructure machines ([https://www.hpci-office.jp/pages/e\\_appli\\_abinit-mp](https://www.hpci-office.jp/pages/e_appli_abinit-mp)).

#### REFERENCES

- (1) Kitaura, K.; Ikeo, E.; Asada, T.; Nakano, T.; Uebayasi, M. Fragment Molecular Orbital Method: An Approximate Computational Method for Large Molecules. *Chem. Phys. Lett.* 1999, 313 (3–4), 701–706.
- (2) Mochizuki, Y.; Tanaka, S.; Fukuzawa, K. Recent Advances of the Fragment Molecular Orbital Method.; Springer Nature Singapore, 2021.

- (3) wwPDB consortium. Protein Data Bank: The Single Global Archive for 3D Macromolecular Structure Data. *Nucleic Acids Res.* 2019, 47 (D1), D520–D528.
- (4) Kitaura, K.; Sugiki, S.-I.; Nakano, T.; Komeiji, Y.; Uebayasi, M. Fragment Molecular Orbital Method: Analytical Energy Gradients. *Chem. Phys. Lett.* 2001, 336 (1–2), 163–170.
- (5) Fedorov, D. G.; Ishida, T.; Uebayasi, M.; Kitaura, K. The Fragment Molecular Orbital Method for Geometry Optimizations of Polypeptides and Proteins. *J. Phys. Chem. A* 2007, 111 (14), 2722–2732.
- (6) Fedorov, D. G.; Alexeev, Y.; Kitaura, K. Geometry Optimization of the Active Site of a Large System with the Fragment Molecular Orbital Method. *J. Phys. Chem. Lett.* 2011, 2 (4), 282–288.
- (7) Tsukamoto, T.; Mochizuki, Y.; Watanabe, N.; Fukuzawa, K.; Nakano, T. Partial Geometry Optimization with FMO-MP2 Gradient: Application to TrpCage. *Chem. Phys. Lett.* 2012, 535, 157–162.
- (8) Mochizuki, Y.; Nakano, T.; Komeiji, Y.; Yamashita, K.; Okiyama, Y.; Yoshikawa, H.; Yamataka, H. Fragment Molecular Orbital-Based Molecular Dynamics (FMO-MD) Method with MP2 Gradient. *Chem. Phys. Lett.* 2011, 504 (1–3), 95–99.
- (9) Tanaka, S.; Mochizuki, Y.; Komeiji, Y.; Okiyama, Y.; Fukuzawa, K. Electron-Correlated Fragment-Molecular-Orbital Calculations for Biomolecular and Nano Systems. *Phys. Chem. Chem. Phys.* 2014, 16 (22), 10310–10344.
- (10) Okamoto, T.; Ishikawa, T.; Koyano, Y.; Yamamoto, N.; Kuwata, K.; Nagaoka, M. A Minimal Implementation of the AMBER-PAICS Interface for Ab Initio FMO-QM/MM-MD Simulation. *BCSJ* 2013, 86 (2), 210–222.

- (11) Nishimoto, Y.; Fedorov, D. G.; Irlle, S. Density-Functional Tight-Binding Combined with the Fragment Molecular Orbital Method. *J. Chem. Theory Comput.* 2014, 10 (11), 4801–4812.
- (12) Nishimoto, Y.; Fedorov, D. G. The Fragment Molecular Orbital Method Combined with Density-Functional Tight-Binding and the Polarizable Continuum Model. *Phys. Chem. Chem. Phys.* 2016, 18 (32), 22047–22061.
- (13) Watanabe, C.; Watanabe, H.; Fukuzawa, K.; Parker, L. J.; Okiyama, Y.; Yuki, H.; Yokoyama, S.; Nakano, H.; Tanaka, S.; Honma, T. Theoretical Analysis of Activity Cliffs among Benzofuranone-Class Pim1 Inhibitors Using the Fragment Molecular Orbital Method with Molecular Mechanics Poisson-Boltzmann Surface Area (FMO+MM-PBSA) Approach. *J. Chem. Inf. Model.* 2017, 57 (12), 2996–3010.
- (14) Okimoto, N.; Otsuka, T.; Hirano, Y.; Taiji, M. Use of the Multilayer Fragment Molecular Orbital Method to Predict the Rank Order of Protein-Ligand Binding Affinities: A Case Study Using Tankyrase 2 Inhibitors. *ACS Omega* 2018, 3 (4), 4475–4485.
- (15) Hatada, R.; Okuwaki, K.; Akisawa, K.; Mochizuki, Y.; Handa, Y.; Fukuzawa, K.; Komeiji, Y.; Okiyama, Y.; Tanaka, S. Statistical Interaction Analyses between SARS-CoV-2 Main Protease and Inhibitor N3 by Combining Molecular Dynamics Simulation and Fragment Molecular Orbital Calculation. *Appl. Phys. Express* 2021, 14, 027003.
- (16) Handa, Y.; Okuwaki, K.; Kawashima, Y.; Hatada, R.; Mochizuki, Y.; Komeiji, Y.; Tanaka, S.; Furuishi, T.; Yonemochi, E.; Honma, T.; Fukuzawa, K. Prediction of Binding Pose and Affinity of Nelfinavir, a SARS-CoV-2 Main Protease Repositioned Drug, by Combining Docking, Molecular Dynamics, and Fragment Molecular Orbital Calculations. *J. Phys. Chem. B* 2024, 128 (10), 2249–2265.

- (17) Takaba, K.; Watanabe, C.; Tokuhisa, A.; Akinaga, Y.; Ma, B.; Kanada, R.; Araki, M.; Okuno, Y.; Kawashima, Y.; Moriwaki, H.; Kawashita, N.; Honma, T.; Fukuzawa, K.; Tanaka, S. Protein–Ligand Binding Affinity Prediction of Cyclin-Dependent Kinase-2 Inhibitors by Dynamically Averaged Fragment Molecular Orbital-Based Interaction Energy. *J. Comput. Chem.* 2022, 43 (20), 1362–1371.
- (18) Tokuda, K.; Watanabe, C.; Okiyama, Y.; Mochizuki, Y.; Fukuzawa, K.; Komeiji, Y. Hydration of Ligands of Influenza Virus Neuraminidase Studied by the Fragment Molecular Orbital Method. *J. Mol. Graph. Model.* 2016, 69, 144–153.
- (19) Fukuzawa, K.; Kitaura, K.; Uebayasi, M.; Nakata, K.; Kaminuma, T.; Nakano, T. Ab Initio Quantum Mechanical Study of the Binding Energies of Human Estrogen Receptor Alpha with Its Ligands: An Application of Fragment Molecular Orbital Method. *J. Comput. Chem.* 2005, 26 (1), 1–10.
- (20) Ishikawa, T.; Yamamoto, N.; Kuwata, K. Partial Energy Gradient Based on the Fragment Molecular Orbital Method: Application to Geometry Optimization. *Chem. Phys. Lett.* 2010, 500 (1–3), 149–154.
- (21) Nakata, H.; Fedorov, D. G. Efficient Geometry Optimization of Large Molecular Systems in Solution Using the Fragment Molecular Orbital Method. *J. Phys. Chem. A* 2016, 120 (49), 9794–9804.
- (22) Nakano, T.; Mochizuki, Y.; Fukuzawa, K.; Amari, S.; Tanaka, S. CHAPTER 2 - Developments and Applications of ABINIT-MP Software Based on the Fragment Molecular Orbital Method. In *Modern Methods for Theoretical Physical Chemistry of Biopolymers*; Starikov, E. B., Lewis, J. P., Tanaka, S., Eds.; Elsevier Science: Amsterdam, 2006; pp 39–52.

- (23) Nakano, T.; Kaminuma, T.; Sato, T.; Fukuzawa, K.; Akiyama, Y.; Uebayasi, M.; Kitaura, K. Fragment Molecular Orbital Method: Use of Approximate Electrostatic Potential. *Chem. Phys. Lett.* 2002, 351 (5–6), 475–480.
- (24) Head, J. D.; Zerner, M. C. A Broyden—Fletcher—Goldfarb—Shanno Optimization Procedure for Molecular Geometries. *Chem. Phys. Lett.* 1985, 122 (3), 264–270.
- (25) Molecular Operating Environment (MOE), 2022.02; Chemical Computing Group ULC, 1010 Sherbrooke St. West, Suite #910, Montreal, QC, Canada, H3A 2R7, 2022
- (26) Halgren, T. A. MMFF VI. MMFF94s Option for Energy Minimization Studies. *J. Comput. Chem.* 1999, 20 (7), 720–729.
- (27) Wang, J.; Cieplak, P.; Kollman, P. A. How Well Does a Restrained Electrostatic Potential (RESP) Model Perform in Calculating Conformational Energies of Organic and Biological Molecules. *J. Comput. Chem.* 2000, 21 (12), 1049–1074.
- (28) Gerber, P. R.; Müller, K. MAB, a Generally Applicable Molecular Force Field for Structure Modelling in Medicinal Chemistry. *J. Comput. Aided Mol.* 1995, 9 (3), 251–268.
- (29) Case, D. A.; Darden, T. A.; Cheatham, T. E.; Simmerling, C. L., Iii; Wang, R, Duke,, J; Luo, M, Crowley,, R; Walker, R. C.; Zhang, W.; Merz, K. M.; Wang, S, Hayik,, B; Roitberg, S. K. A.; Wong, K. F.; Paesani, F.; Vanicek, J.; Wu, X.; Brozell, S. R.; Steinbrecher, T.; Gohlke, H.; Yang, L.; Tan, C.; Mongan, J.; Hornak, V.; Cui, G.; Mathews, D. H.; Seetin, M. G.; Sagui, C.; Kollman, V. B. A. P. A. K. *AMBER 10*; infoscience.epfl.ch: San Francisco, 2008.
- (30) Mochizuki, Y.; Yamashita, K.; Murase, T.; Nakano, T.; Fukuzawa, K.; Takematsu, K.; Watanabe, H.; Tanaka, S. Large Scale FMO-MP2 Calculations on a Massively Parallel-Vector Computer. *Chem. Phys. Lett.* 2008, 457 (4–6), 396–403.

- (31) Okiyama, Y.; Nakano, T.; Yamashita, K.; Mochizuki, Y.; Taguchi, N.; Tanaka, S. Acceleration of Fragment Molecular Orbital Calculations with Cholesky Decomposition Approach. *Chem. Phys. Lett.* 2010, 490 (1), 84–89.
- (32) Watanabe, C.; Watanabe, H.; Okiyama, Y.; Takaya, D.; Fukuzawa, K.; Tanaka, S.; Honma, T. Development of an Automated Fragment Molecular Orbital (FMO) Calculation Protocol toward Construction of Quantum Mechanical Calculation Database for Large Biomolecules. *Chem-Bio Inf. J.* 2019, 19 (0), 5–18.
- (33) Takaya, D.; Watanabe, C.; Nagase, S.; Kamisaka, K.; Okiyama, Y.; Moriwaki, H.; Yuki, H.; Sato, T.; Kurita, N.; Yagi, Y.; Takagi, T.; Kawashita, N.; Takaba, K.; Ozawa, T.; Takimoto-Kamimura, M.; Tanaka, S.; Fukuzawa, K.; Honma, T. FMO DB: The World's First Database of Quantum Mechanical Calculations for Biomacromolecules Based on the Fragment Molecular Orbital Method. *J. Chem. Inf. Model.* 2021, 61 (2), 777–794.
- (34) Fukuzawa, K.; Watanabe, C. Application of the FMO method using ABINIT-MP/BioStation for drug discovery. *CICSJ Bulletin* 2013, 31 (4), 89.
- (35) Mochizuki, Y.; Yamashita, K.; Fukuzawa, K.; Takematsu, K.; Watanabe, H.; Taguchi, N.; Okiyama, Y.; Tsuboi, M.; Nakano, T.; Tanaka, S. Large-Scale FMO-MP3 Calculations on the Surface Proteins of Influenza Virus, Hemagglutinin (HA) and Neuraminidase (NA). *Chem. Phys. Lett.* 2010, 493 (4–6), 346–352.
- (36) Nakano, H.; Saito, N.; Parker, L.; Tada, Y.; Abe, M.; Tsuganezawa, K.; Yokoyama, S.; Tanaka, A.; Kojima, H.; Okabe, T.; Nagano, T. Rational Evolution of a Novel Type of Potent and Selective Proviral Integration Site in Moloney Murine Leukemia Virus Kinase 1 (PIM1) Inhibitor from a Screening-Hit Compound. *J. Med. Chem.* 2012, 55 (11), 5151–5164.

Graphical Abstract

